Valence band offsets for ALD SiO_2 and Al_2O_3 on $(In_xGa_{1-x})_2O_3$ for x = 0.25–0.74

Chaker Fares (iD), Max Kneiß (iD), Holger von Wenckstern (iD), Marius Grundmann (iD), Marko Tadjer, Fan Ren (iD), Eric Lambers (iD), and S. J. Pearton (iD)

View Online   Export Citation   CrossMark

AIP Publishing

Valence band offsets for ALD SiO₂ and Al₂O₃ on (InₓGa₁₋ₓ)₂O₃ for x = 0.25–0.74

Chaker Fares,[1] (iD) Max Kneiß,[2] (iD) Holger von Wenckstern,[2] (iD) Marius Grundmann,[2] (iD) Marko Tadjer,[3]
Fan Ren,[1] (iD) Eric Lambers,[4] and S. J. Pearton[5] (iD)

AFFILIATIONS

[1] Department of Chemical Engineering, University of Florida, Gainesville, Florida 32611, USA

[2] Universität Leipzig, Felix-Bloch-Institut für Festkörperphysik, 04103 Leipzig, Germany

[3] U.S. Naval Research Laboratory, Washington, DC 20375, USA

[4] Nanoscale Research Facility, University of Florida, Gainesville, Florida 32611, USA

[5] Department of Materials Science and Engineering, University of Florida, Gainesville, Florida 32611, USA

ABSTRACT

The incorporation of In₂O₃ into Ga₂O₃ allows for tailoring of the bandgap over a wide range in (InₓGa₁₋ₓ)₂O₃, and this material is emerging as a candidate in transparent electrodes on optoelectronic devices, heterostructure transistors, photodetectors, and gas sensors. We have measured the band alignments for atomic layer deposited SiO₂ and Al₂O₃ over the composition range x = 0.25–0.74 for (InₓGa₁₋ₓ)₂O₃ grown by pulsed laser deposition. The valence band offsets from 1.95 to 2.30 eV for SiO₂ and 0.88 to 1.23 eV for Al₂O₃ over this composition range. The bandgaps of (InₓGa₁₋ₓ)₂O₃ spanned from 4.55 to 4.05 for x = 0.74–0.25. This led to nested band alignments for SiO₂ and Al₂O₃ for the entire composition range of (InₓGa₁₋ₓ)₂O₃ investigated.

INTRODUCTION

Solid solutions between the binary transparent oxides In₂O₃ and Ga₂O₃ are of interest in establishing miscibility gaps, the behavior of charge accumulation layers, and native defect behavior as the cubic symmetry In₂O₃ is alloyed with the monoclinic Ga₂O₃.[1–24] Alloys of indium and gallium oxides were reported for the rhombohedral α-phase, the cubic bixbyite phase, and the monoclinic β-phase.[1–4,7–9] There have been several reviews of the crystal structures and phase stability of (InₓGa₁₋ₓ)₂O₃, which can show 4-, 5-, or 6-fold coordinated cation sites.[1,8] The ability to tune the wavelength response of photodetectors and the mobility and carrier confinement in heterostructure transistors based on the (InₓGa₁₋ₓ)₂O₃ system offer new possibilities in these technologies.[1,8,13,14,21,25] For example, it is expected that a two-dimensional electron gas of high sheet carrier density can be induced by the polarization differences at ε-(In,Ga)₂O₃/ε-(Al,Ga)₂O₃ heterointerfaces.[11] A variety of synthesis methods for this ternary system have been reported, including molecular beam epitaxy, metal organic chemical vapor deposition, sputtering, pulsed laser

deposition (PLD), and sol-gel processing, each presenting different phase stabilities.[1,3,5,8,13,15,21–32]

An important aspect for any of these applications is the band alignment of the alloys with common dielectrics used for MOS gates on transistors or surface passivation. For carrier confinement in MOS transistors, the conduction and valence band offsets (VBOs) should be ideally >1 eV.[33] Figure 1 shows a compilation of bandgaps for common dielectrics, along with the expected range of bandgaps for (InₓGa₁₋ₓ)₂O₃ with x = 0–0.7. Two attractive options are SiO₂, with its large gap and well-established deposition conditions, and Al₂O₃—both of these are readily deposited by Atomic Layer Deposition (ALD), which provides a controlled, low damage process. While there have been numerous reports on band alignments for different dielectrics on (AlₓGa₁₋ₓ)₂O₃,[34–36] there are few comparable studies on (InₓGa₁₋ₓ)₂O₃ in part due to the difficulty in preparing high quality samples.

In this paper, we report on the measurement of valence band offsets for ALD SiO₂ and Al₂O₃ on (InₓGa₁₋ₓ)₂O₃ for x = 0.25–0.74, obtained by X-Ray Photoelectron Spectroscopy (XPS). The samples were grown by continuous composition spread

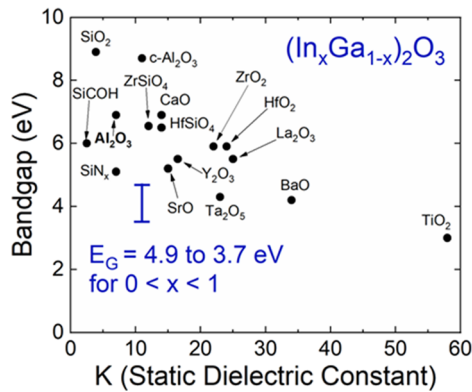FIG. 1. Dielectric constant and bandgap of candidate dielectrics on $(In_xGa_{1-x})_2O_3$.

PLD.[1,8,28–31] The bandgaps of the $(In_xGa_{1-x})_2O_3$ were measured from the photoemission spectra, and this allowed derivation of the conduction band offsets for both dielectrics. The band alignments are nested (type I) in both cases, with valence band offsets
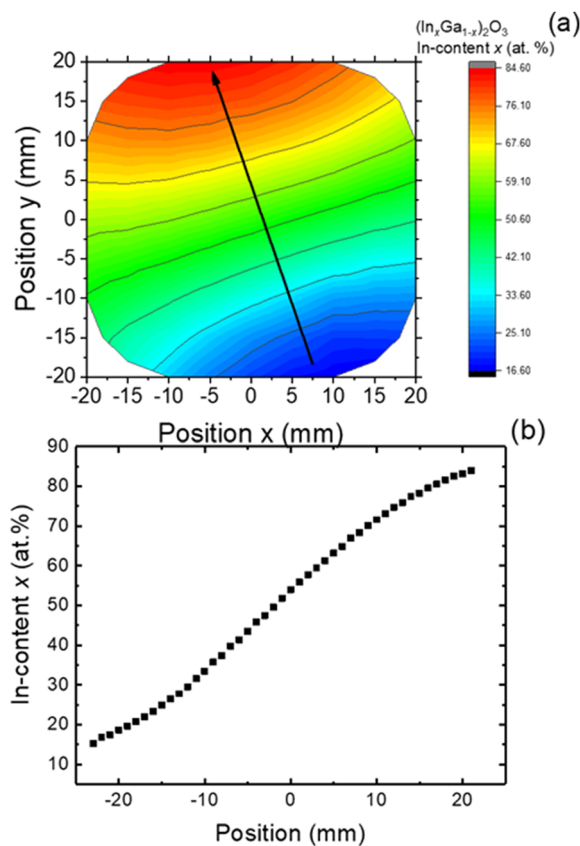
FIG. 2. (a) False-color representation of the In concentration within a 2 in. diameter $(In_{1-x}Ga_x)_2O_3$ thin film grown with continuously varying composition on (100) MgO and (b) line scan of In content as a function of position along the wafer determined by EDX. The scan was obtained along the gradient direction depicted with black arrow in (a).
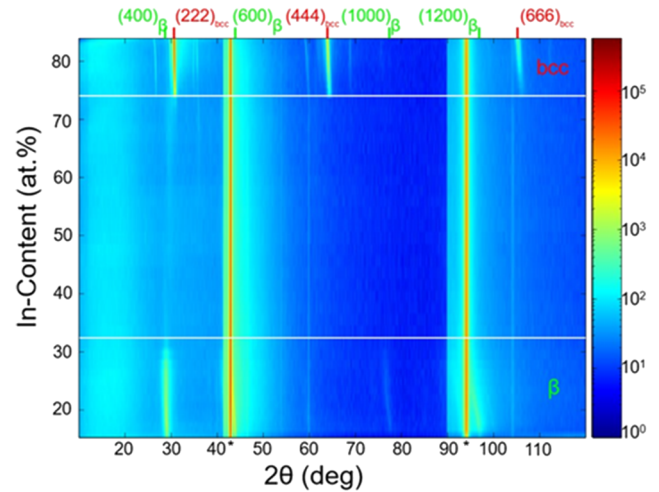
FIG. 3. False-color representation of θ–2θ X-ray diffractograms acquired along the compositional gradient of an $(In_xGa_{1-x})_2O_3$ CCS-PLD sample deposited on (100) MgO substrates at about 650 °C. Peaks labeled β belong to the monoclinic Ga_2O_3 phase, while bcc denotes reflections of the cubic bixbyite In_2O_3 structure. Intense peaks marked with an asterisk are due to the (100) MgO substrate. No thin film reflections occur in the composition range between the white solid lines corresponding to X-ray amorphous growth.
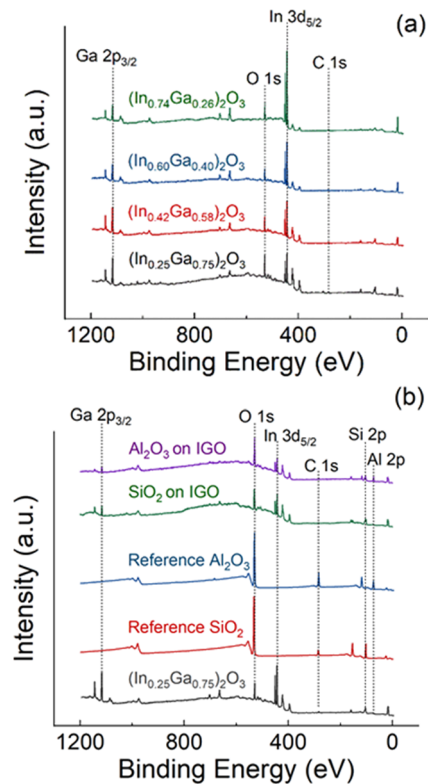
FIG. 4. XPS survey scans of (a) $(In_xGa_{1-x})_2O_3$ at the indium concentrations studied in this report and (b) thick ALD Al_2O_3, thick ALD SiO_2, and heterostructures of each oxide on IGO. The intensity is in arbitrary units (a.u.).
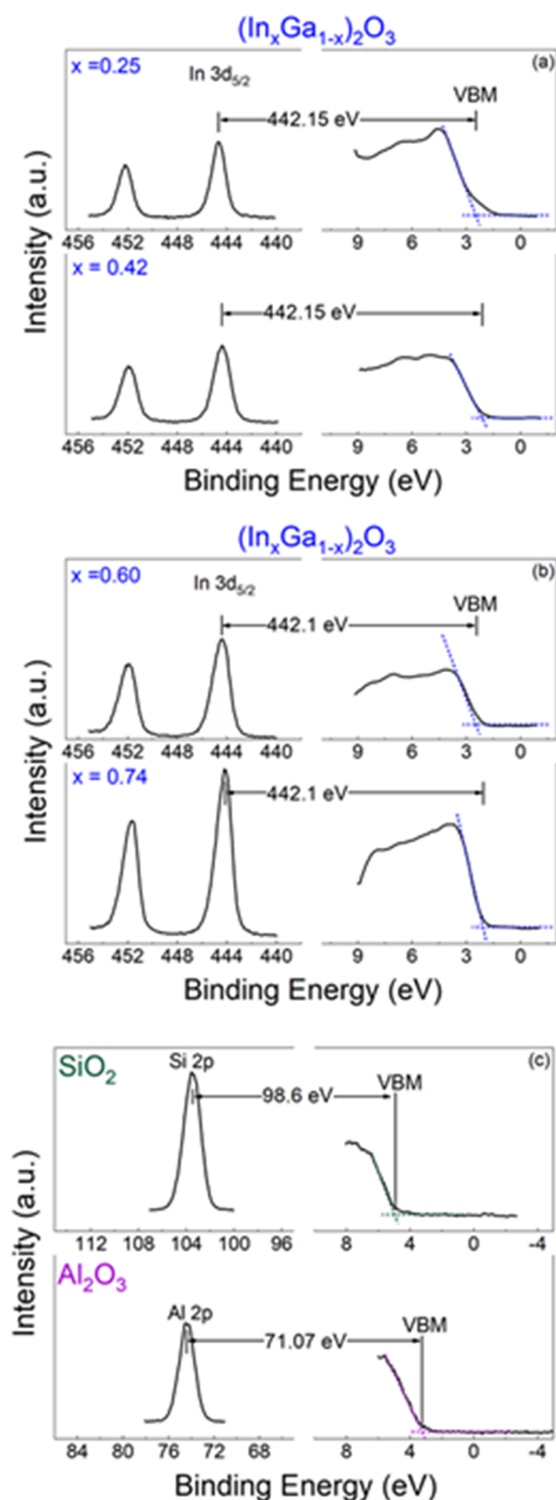
FIG. 5. XPS spectra of core levels to the valence band maximum (VBM) for (a) reference $(In_xGa_{1-x})_2O_3$ with 25% and 42% indium, (b) reference $(In_xGa_{1-x})_2O_3$ with 60% and 74% indium, and (c) thick ALD films Al_2O_3 and SiO_2. The intensity is in arbitrary units (a.u.).
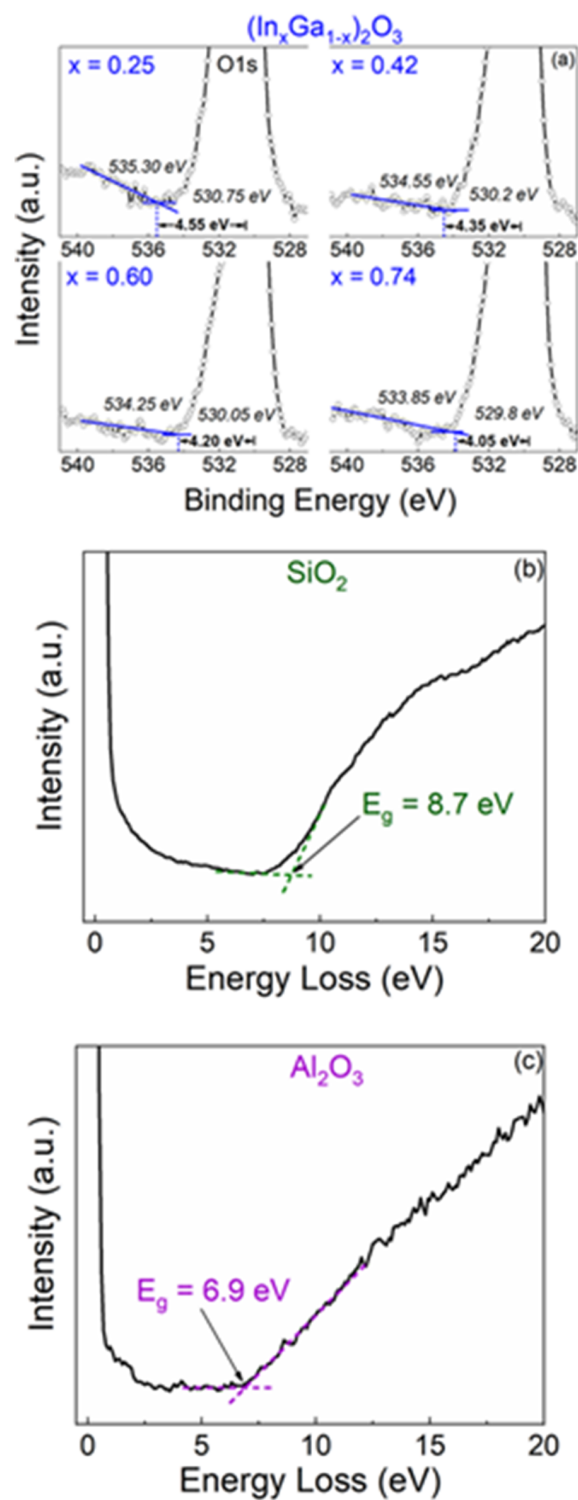
FIG. 6. Bandgap of (a) $(In_xGa_{1-x})_2O_3$ determined using the onset of the plasmon loss feature in the O 1s photoemission spectrum and (b) ALD SiO_2 and (c) ALD Al_2O_3 where both deposited films' bandgap was determined by reflection electron energy loss spectra. The intensities are in arbitrary units (a.u.).

1.95–2.30 eV for SiO_2 and 0.88–1.23 eV for Al_2O_3 over the composition range we investigated.

EXPERIMENTAL

The continuous composition spread PLD technique was used to grow $(In_xGa_{1-x})_2O_3$ thin films using a target consisting of semicircular In_2O_3 and Ga_2O_3 segments.[1,8,28–31,37–39] The sample was deposited at a growth temperature of 650 °C and an oxygen pressure of 0.08 mbar on a 2 in. diameter (100) MgO substrate. The indium concentration varied between 0.16 and 0.86 and showed a slight S-shaped dependence along the gradient direction, in agreement with calculation.[29] Along lines perpendicular to the gradient direction, the In concentration was constant. Energy-dispersive X-ray spectroscopy (EDX) was used for the spatially resolved chemical analysis.[8,29] Figure 2 shows the variation of In content as both a compositional map (a) and a lateral line scan (b). Detailed characterization of similar films is discussed elsewhere.[1,3,8] Figure 3 shows a false color representation of x-ray diffractograms along the compositional gradient. The monoclinic phase is dominant for Ga-rich compositions, with (100) oriented growth, while for In-rich conditions, the (111) oriented cubic bixbyite phase is predominant.[3] Four sections from this sample with composition x = 0.25, 0.42, 0.60, and 0.74 determined by XPS were diced to provide specific compositions for dielectric ALD. The sample positions were identified with alignment marks in a photoresist and mapped to the compositional data. The uncertainty in the spatial correlation was less than 50 μm after dicing. This corresponds to a compositional variation of ±2% in absolute value. Note that for x > 0.75 (z > 15 mm), the sample

has a cubic bixbyite structure, but we did not investigate if there was a systematic change of bandgap as the Ga-content in the cubic phase decreased in order to avoid edge effects in the samples.

The ALD layers were deposited at 200 °C in a remote plasma mode in a Cambridge Nano Fiji 200 using a trimethylaluminum precursor or Tris(dimethylamino)silane and an inductively coupled plasma (ICP) at 300 W to generate atomic oxygen.[34,35] For substrate cleaning prior to deposition, a rinse sequence consisting of acetone and IPA was followed by drying in filtered N_2 and finally ozone exposure for 15 min. After this substrate cleaning, samples were directly loaded into the deposition systems within a cleanroom environment to avoid contamination of the deposited films. Both thick (200 nm) and thin (1.5 nm) layers of the dielectrics were deposited for measuring both bandgaps and core levels on the $(In_xGa_{1-x})_2O_3$.

We used XPS survey scans to establish the chemical state of the SiO_2, Al_2O_3, and $(In_xGa_{1-x})_2O_3$ samples.[40] The XPS system was a Physical Instruments ULVAC PHI, with an Al x-ray source (energy 1486.6 eV, source power 300 W), an analysis size of 100 μm diameter, a take-off angle of 50°, and an acceptance angle of ±7°. The electron pass energy was 23.5 eV for high-resolution scans and 93.5 eV for survey scans. The total energy resolution of this XPS system is about 0.5 eV, and the accuracy of the observed binding energy is within 0.03 eV. The most common method of measuring the valence band offset involves using X-ray photoelectron spectroscopy (XPS) to measure the core levels of a system.[40] The basic method is to first measure the energy difference between a core level and the valence band maximum (VBM) for both a single layer dielectric and the $(In_xGa_{1-x})_2O_3$.[40]
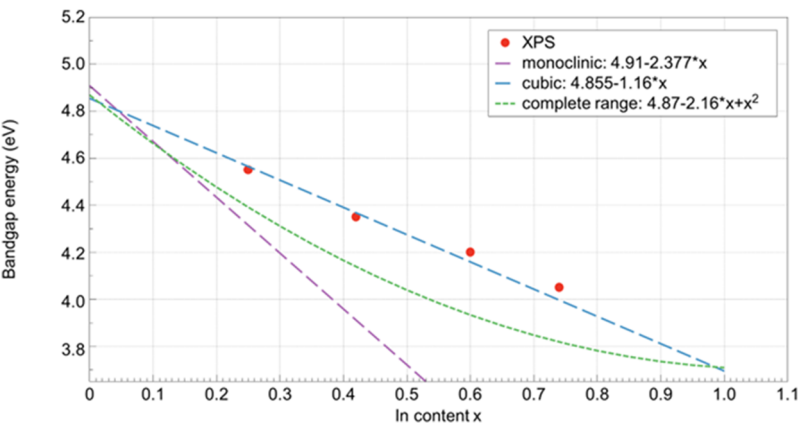
FIG. 7. Variation of bandgap determined by XPS, showing good fits to the cubic phase. The results expected from monoclinic and the bowing reported over the large composition range are also shown. Reference 1 has a full discussion of the effects of how bandgap was determined and the impact of different growth methods.

TABLE I. Summary of the measured reference and heterostructure peaks for SiO_2 on $(In_xGa_{1-x})_2O_3$ (eV).

Indium concentration	Reference $(In_xGa_{1-x})_2O_3$			Reference SiO_2			Thin SiO_2 on $(In_xGa_{1-x})_2O_3$	
	Core level peak (In $3d_{5/2}$)	VBM	Core-VBM	Core level peak (in Si $2p$)	VBM	Core-VBM	Δ core level (In $3d_{5/2}$-Si $2p$)	Valence band offset
$(In_{0.25}Ga_{0.75})_2O_3$	444.65	2.50 ± 0.15	442.15	103.40	4.80	98.60	341.60	1.95
$(In_{0.42}Ga_{0.58})_2O_3$	444.40	2.25 ± 0.15	442.15	...	...	...	341.45	2.10
$(In_{0.60}Ga_{0.40})_2O_3$	444.35	2.25 ± 0.15	442.10	...	...	...	341.30	2.20
$(In_{0.74}Ga_{0.26})_2O_3$	444.20	2.10 ± 0.15	442.10	...	...	...	341.20	2.30

TABLE II. Summary of the measured reference and heterostructure peaks for Al_2O_3 on $(In_xGa_{1-x})_2O_3$ (eV).

Indium concentration	Reference $(In_xGa_{1-x})_2O_3$			Reference Al_2O_3			Thin Al_2O_3 on $(In_xGa_{1-x})_2O_3$	
	Core level peak (In $3d_{5/2}$)	VBM	Core-VBM	Core level peak (in Al 2p)	VBM	Core-VBM	Δ core level (In $3d_{5/2}$-Al 2p)	Valence band offset
$(In_{0.25}Ga_{0.75})_2O_3$	444.65	2.50 ± 0.15	442.15	74.32	3.25	71.07	370.20	0.88
$(In_{0.42}Ga_{0.58})_2O_3$	444.40	2.25 ± 0.15	442.15	. . .	. . .	. . .	370.10	0.98
$(In_{0.60}Ga_{0.40})_2O_3$	444.35	2.25 ± 0.15	442.10	. . .	. . .	. . .	369.90	1.13
$(In_{0.74}Ga_{0.26})_2O_3$	444.20	2.10 ± 0.15	442.10	. . .	. . .	. . .	369.80	1.23

Heterojunction samples, consisting of the thin (1.5 nm) layer of dielectric deposited on the $(In_xGa_{1-x})_2O_3$, were then prepared in which the separation between reference core levels in each material is measured.[40] The separation between the reference core levels can be translated directly into a value for the valence band offset (VBO) using the previously measured single layer sample core-level to VBM energies. The primary source of uncertainty in XPS measurements of band offsets arises from determining the position of the valence band maximum. The most used method produces a highly precise technique by linearly fitting
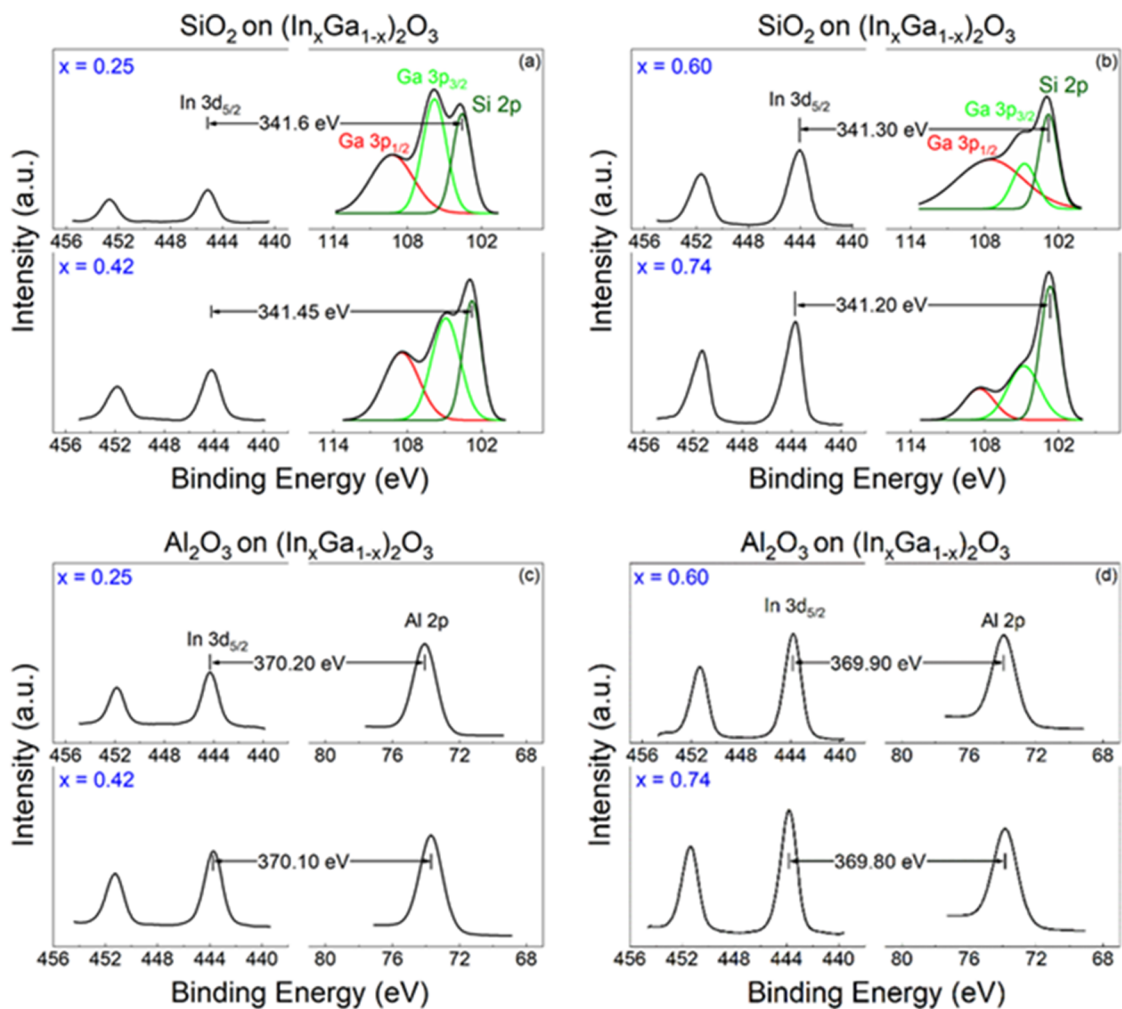
FIG. 8. High resolution XPS spectra for [(a) and (b)] the $(In_xGa_{1-x})_2O_3$ to SiO_2 core delta regions and [(c) and (d)] the $(In_xGa_{1-x})_2O_3$ to Al_2O_3 core delta regions. The intensity is in arbitrary units (a.u.).

the leading edge of the valence electron spectrum to the flat band energy.

To avoid sample charging, charge compensation employed an electron flood gun and a simultaneous ion beam. C 1s core levels of the surface adsorbate (284.8 eV) were used to calibrate the binding energy.[33] Only the relative energy position is needed to determine the valence band offsets, so the absolute energy calibration for a sample has no effect on that number. The samples were electrically insulated from the chuck to avoid uneven charge dispersion along the sample. All electron analyzers and equipment were grounded. Differential charging was not observed in any of the samples with the use of the electron gun. The SiO_2 and Al_2O_3 bandgaps were obtained from Reflection Electron Energy Loss Spectroscopy (REELS)[41,42] using a 1 kV electron beam and hemispherical electron analyzer. The bandgaps of the $(In_xGa_{1−x})_2O_3$ for each composition were obtained from XPS energy loss measurements of the O 1s peak.[43]

RESULTS AND DISCUSSION

XPS survey scans from the four different compositions of $(In_xGa_{1−x})_2O_3$ are shown in Fig. 4(a), and all of them show only the lattice constituents being present. The survey spectra for the thick (200 nm) dielectrics of ALD SiO_2 and Al_2O_3 and thin (1.5 nm) dielectrics of ALD SiO_2 and Al_2O_3 on $(In_xGa_{1−x})_2O_3$, labeled IGO, and the $(In_{0.24}Ga_{0.76})_2O_3$ sample for reference are shown in Fig. 4(b).

The high resolution XPS spectra for the vacuum-core delta regions of $(In_xGa_{1−x})_2O_3$ with x = 0.25 and 0.42 are shown in Fig. 5(a), $(In_xGa_{1−x})_2O_3$ with x = 0.60 and 0.74 in Fig. 5(b), and the SiO_2 and Al_2O_3 in Fig. 5(c). As discussed earlier, the valence band offsets are extracted from the shift of the core levels for the heterostructure samples with the thin dielectric on top of different compositions of $(In_xGa_{1−x})_2O_3$.[34,35,43] Once the valence band offsets are known, to determine the conduction band offset, it is necessary to measure the bandgap of each composition. We measured the bandgaps of the four $(In_xGa_{1−x})_2O_3$ compositions, as shown in Fig. 6(a), from the separation between the core level peak energy and the onset of inelastic (plasmon) losses in each O 1s photoemission spectrum.[36] To find the band-gap energy, a linear fit is made to the measured loss spectrum curve near the approximate location of onset of inelastic losses. Next, by subtracting the background, the "zero" level is determined. The energy corresponding to the onset of inelastic losses is found by extrapolating the linear-fit line and calculating its intersection with the "zero" level.[33,40] The bandgap energy is equal to the difference between the core-level peak energy and the onset of inelastic losses. The respective bandgaps were 4.55 eV for $(In_{0.25}Ga_{0.75})_2O_3$, 4.35 eV for $(In_{0.42}Ga_{0.58})_2O_3$, 4.20 eV for $(In_{0.60}Ga_{0.40})_2O_3$, and 4.05 eV for $(In_{0.74}Ga_{0.26})_2O_3$. These are in general agreement with the reported values for PLD films in a similar composition range.[1,8] A compilation of values obtained for different growth methods and conditions is given elsewhere.[1,8,12] Figure 6(b) shows the REELS spectra to determine the bandgap of the SiO_2 and Al_2O_3, with values of 8.7 eV and 6.9 eV, respectively. These are consistent with previously reported values.[34–36]

Figure 7 shows that the bandgaps determined by XPS follow the relation $E_G = 4.855 − 1.16x$, where x is the In composition in these cubic films. von Wenckstern[1,8] has given a detailed discussion of the effect of the growth method, phase, and technique in
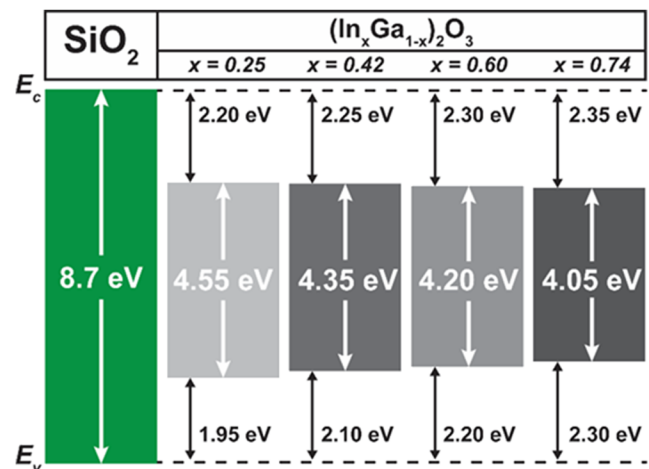

FIG. 9. Band diagrams for the $SiO_2/(In_xGa_{1−x})_2O_3$ heterostructure in which the SiO_2 was deposited by ALD.

determining bandgaps on the compositional dependence of bandgaps in $(In,Ga)_2O_3$ films.

Tables I and II show the valence band maximum (VBM) for the SiO_2 and Al_2O_3 and the $(In_xGa_{1−x})_2O_3$ from linear fitting of the leading edge of the valence band. The XPS spectra from which we extracted the core energy differences as a function of Al composition are shown in Fig. 8. The core energy levels and the differences between Ga 2p3/2 and Si 2p or Al 2p core energy levels, respectively, are shown in the figure. The corresponding VBMs were 2.5 ± 0.15 eV for $(In_{0.25}Ga_{0.76})_2O_3$, 2.25 ± 0.15 eV for $(In_{0.42}Ga_{0.58})_2O_3$, 2.25 ± 0.15 eV for $(In_{0.60}Ga_{0.40})_2O_3$, and 2.10 ± 0.15 eV for $(In_{0.74}Ga_{0.26})_2O_3$. The error bars in different binding energies were combined in a root sum square relationship to determine the overall error bars in the valence band offsets.[33] The valence band offsets for SiO_2 were 1.95 ± 0.30 eV for $(In_{0.25}Ga_{0.75})_2O_3$, 2.10 ± 0.30 eV for $(In_{0.42}Ga_{0.58})_2O_3$, 2.20 ± 0.30 eV for $(In_{0.60}Ga_{0.40})_2O$,
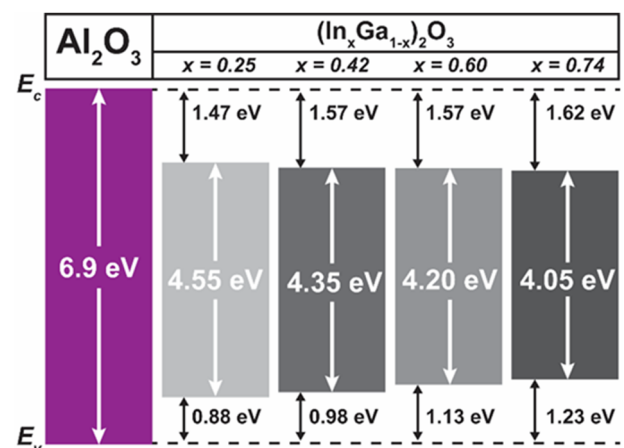

FIG. 10. Band diagrams for the $Al_2O_3/(In_xGa_{1−x})_2O_3$ heterostructure in which the Al_2O_3 was deposited by ALD.

and 2.30 ± 0.35 eV for $(In_{0.74}Ga_{0.26})_2O_3$. The conduction band offsets were then 2.20 eV (x = 0.25), 2.25 eV (x = 0.42), 2.30 eV (x = 0.6), and 2.30 eV (x = 0.74). SiO_2 therefore provides excellent confinement of electrons in $(In_xGa_{1-x})_2O_3$ samples over the entire composition range, and the $SiO_2/In_xGa_{1-x})_2O_3$ band alignment is type I, as shown in the schematic of Fig. 9.

The valence band offsets for Al_2O_3 were 0.88 ± 0.20 eV for $(In_{0.25}Ga_{0.75})_2O_3$, 0.98 ± 0.20 eV for $(In_{0.42}Ga_{0.58})_2O_3$, 1.13 ± 0.25 eV for $(In_{0.60}Ga_{0.40})_2O_3$, and 1.23 ± 0.25 eV for $(In_{0.74}Ga_{0.26})_2O_3$. Based on the measured bandgap of Al_2O_3, the conduction band offsets were then 1.47 eV (x = 0.25), 1.57 eV (x = 0.42), 1.57 eV (x = 0.60), and 1.62 eV (x = 0.74). The band alignments are also type I, as shown in the schematic of Fig. 10. Basically, both the conduction and valence band offsets are adequate for good carrier confinement for both dielectrics at all compositions of $(In_xGa_{1-x})_2O_3$.

SUMMARY AND CONCLUSIONS

The valence band offsets of $SiO_2/(In_xGa_{1-x})_2O_3$ and $Al_2O_3/(In_xGa_{01-x})_2O_3$ heterojunctions were measured over a range of In contents (x = 0.25–0.74). The band alignments are type I in all cases, with valence band offsets >1.95 eV for SiO_2 and >0.88 eV for Al_2O_3 across the composition range of $(In_xGa_{1-x})_2O_3$ examined. Both of these common dielectrics will provide effective carrier confinement in heterostructures with $(In_xGa_{01-x})_2O_3$. Future work should examine the thermal stability and interface state densities of these systems.

ACKNOWLEDGMENTS

REFERENCES

[1] H. von Wenckstern, Adv. Electron. Mater. **3**, 1600350 (2017).
[2] F. Fuchs and F. Bechstedt, Phys. Rev. B **77**, 155107 (2008).
[3] C. Kranert, J. Lenzner, J. Marcus, M. Lorenz, H. von Wenckstern, R. Schmidt-Grund, and M. Grundmann, J. Appl. Phys. **116**, 013505 (2014).
[4] G. Patzke and M. Binnewies, Solid State Sci. **2**, 689 (2000).
[5] J. M. Phillips, J. Kwo, G. A. Thomas, S. A. Carter, R. J. Cava, and S. Y. Hou, "Transparent conducting thin films of GaInO₃," Appl. Phys. Lett. **65**, 115 (1994).
[6] C. Janowitz, V. Scherer, M. Mohamed, A. Krapf, H. Dwelk, R. Manzke, Z. Galazka, R. Uecker, K. Irmscher, R. Fornari, M. Michling, D. Schmeißer, J. R. Weber, J. B. Varley, and C. G. Van de Walle, New J. Phys. **13**, 085014 (2011).
[7] R. Schmidt-Grund, C. Kranert, T. Böntgen, H. von Wenckstern, H. Krauß, and M. Grundmann, J. Appl. Phys. **116**, 053510 (2014).
[8] H. von Wenckstern, "Properties of (In,Ga)₂O₃ alloys," in Gallium Oxide Technology, Devices and Applications, edited by S. Pearton, F. Ren, and M. Mastro (Elsevier, Oxford, 2018).
[9] D. D. Edwards, P. E. Folkins, and T. O. Mason, J. Am. Ceramic Soc. **80**, 253 (1997).
[10] V. Wang, W. Xiao, D. M. Ma, R.-J. Liu, and C. M. Yang, J. Appl. Phys. **115**, 043708 (2014).
[11] M. B. Maccioni and V. Fiorentini, Appl. Phys. Express **9**, 041102 (2016).
[12] H. Peelaers, D. Steiauf, J. Varley, A. Janotti, and C. G. V. Walle, Phys. Rev. B **92**, 085206 (2015).
[13] F. Zhang, H. Li, M. Arita, and Q. Guo, Opt. Mater. Express **7**, 3769 (2017).
[14] Z. Zhang, H. Wenckstern, J. Lenzner, M. Lorenz, and M. Grundmann, Appl. Phys. Lett. **108**, 123503 (2016).
[15] X. Wang, Z. Chen, K. Saito, T. Tanaka, M. Nishio, and Q. Guo, J. Alloys Compd. **690**, 287 (2017).
[16] P. D. C. King, T. D. Veal, D. J. Payne, A. Bourlange, R. D. Egdell, and C. F. McConville, Phys. Rev. Lett. **101**, 116808 (2008).
[17] F. Yang, J. Ma, C. Luan, and L. Kong, Appl. Surf. Sci. **255**, 4401 (2009).
[18] M. Baldini, M. Albrecht, D. Gogova, R. Schewski, and G. Wagner, Semicond. Sci. Technol. **30**, 024013 (2015).
[19] P. Vogt and O. Bierwagen, APL Mater. **4**, 086112 (2016).
[20] T. Oshima and S. Fujita, Phys. Stat. Solidi C **5**, 3113 (2008).
[21] Y. Kokubun, T. Abe, and S. Nakagomi, Phys. Status Solidi A **207**, 1741 (2010).
[22] T. Minami, Y. Takeda, T. Kakumu, S. Takata, and I. Fukuda, J. Vac. Sci. Technol., A **15**, 958 (1997).
[23] A. Wang, N. L. Edleman, J. R. Babcock, and T. J. Marks, J. Mater. Res. **17**, 3155 (2002).
[24] M. Grundmann, H. Frenzel, A. Lajn, M. Lorenz, F. Schein, and H. von Wenckstern, Phys. Stat. Solidi A **207**, 1437 (2010).
[25] F. Zhang, K. Saito, T. Tanaka, M. Nishio, and Q. Guo, Solid State Commun. **186**, 28 (2014).
[26] W.-T. Lin, C.-Y. Ho, Y.-M. Wang, K.-H. Wu, and W.-Y. Chou, J. Phys. Chem. Solids **73**, 948 (2012).
[27] F. Zhang, K. Saito, T. Tanaka, M. Nishio, and Q. Guo, J. Alloys Compd. **614**, 173 (2014).
[28] M. Kneiß, P. Storm, G. Benndorf, M. Grundmann, and H. von Wenckstern, ACS Comb. Sci. **20**, 643 (2018).
[29] H. von Wenckstern, Z. Zhang, F. Schmidt, J. Lenzner, H. Hochmuth, and M. Grundmann, Cryst. Eng. Commun. **15**, 10020 (2013).
[30] H. von Wenckstern, D. Splith, A. Werner, S. Müller, M. Lorenz, and M. Grundmann, ACS Comb. Sci. **17**, 710 (2015).
[31] H. von Wenckstern, D. Splith, M. Purfürst, Z. Zhang, C. Kranert, S. Müller, M. Lorenz, and M. Grundmann, Semicond. Sci. Technol. **30**, 024005 (2015).
[32] D. C. Hays, B. P. Gila, S. J. Pearton, and F. Ren, Appl. Phys. Rev. **4**, 021301 (2017).
[33] Z. Feng, F. Qian, J. Zhang, C. Zhang, H. Zhou, L. Xiang, L. Huang, L. Xu, Y. Hu, S. Zhao, and H. Yue, J. Alloys Compd. **745**, 292 (2018).
[34] C. Fares, F. Ren, E. S. Lambers, D. C. Hays, B. P. Gila, and S. J. Pearton, J. Electron. Mater. **48**, 1568 (2019).
[35] C. Fares, F. Ren, E. Lambers, D. C. Hays, B. P. Gila, and S. J. Pearton, Semicond. Sci. Technol. **34**, 025006 (2019).
[36] C. Fares, F. Ren, E. Lambers, D. C. Hays, B. P. Gila, and S. J. Pearton, J. Vac. Sci. Technol. B **36**, 061207 (2018).
[37] M. Lorenz, H. Hochmuth, H. Hilmer, A. Lajn, D. Spemann, M. Brandt, J. Zippel, R. Schmidt-Grund, H. von Wenckstern, and M. Grundmann, Laser Chem. **2010**, 140976.
[38] A. Hassa, H. von Wenckstern, D. Splith, C. Sturm, M. Kneiß, V. Prozheeva, and M. Grundmann, APL Mater. **7**, 022525 (2019).
[39] M. Kneiß, A. Hassa, D. Splith, C. Sturm, H. von Wenckstern, T. Schultz, N. Koch, M. Lorenz, and M. Grundmann, APL Mater. **7**, 022516 (2019).
[40] E. A. Kraut, R. W. Grant, J. R. Waldrop, and S. P. Kowalczyk, Phys. Rev. Lett. **44**, 1620 (1980).
[41] E. Bersch, M. Di, S. Consiglio, R. D. Clark, G. J. Leusink, and A. C. Diebold, J. Appl. Phys. **107**, 043702 (2010).
[42] H. C. Shin, D. Tahir, S. Seo, Y. R. Denny, S. K. Oh, H. J. Kang, S. Heo, J. G. Chung, J. C. Lee, and S. Tougaard, Surf. Interface Anal. **44**, 623 (2012).
[43] C. Fares, F. Ren, E. Lambers, D. C. Hayes, B. P. Gila, and S. J. Pearton, ECS J. Solid State Sci. Technol. **7**, P519 (2018).